Wireless Power Transfer Utilizing a High-Q Self-Resonant Structure

Aaron L. F. Stein, Phyo Aung Kyaw, *Student Member, IEEE*, and Charles R. Sullivan, *Fellow, IEEE*

***Abstract*—The range and efficiency of a wireless power transfer (WPT) system is limited by the quality factor of the resonant coils. Conventional resonant coils are made from solid or Litz wire. At megahertz frequencies solid wire is not utilized well due to skin effect, and Litz wire is very lossy due to proximity effect. We present a multilayer self-resonant structure as a low-cost method for creating high-Q coils. This structure uses thin foil layers that are separated by a dielectric material in order to form an LC resonator, while also forcing equal current sharing between conductors. The self-resonant structure makes it feasible to achieve advantages similar to Litz wire, but at multi-megahertz frequencies where effective Litz wire is not commercially available. These structures are made with foil layers much thinner than a skin depth, which can make handling these thin layers a challenge. To solve this problem, we also present a modified self-resonant structure in which the layered conductors are made with flex-PCB substrates with no vias. The PCB substrates provide a relatively inexpensive way to handle thin conductive layers, and the modified self-resonant structure ensures that the poor dielectric properties of the PCB substrates do not impact the quality factor of the structure. A prototype of the modified self-resonant structure has a quality factor of 1183 at 7.09 MHz, despite only being 6.6 cm in diameter, which is more than 6.5x larger than other coils presented in the literature with a similar diameter. An experimental WPT setup utilizing two self-resonant structures achieves 94% efficiency at a distance of 5.0 cm, which is more than twice the distance as similarly sized conventional coils can achieve while maintaining the same efficiency.**

***Index Terms*—Eddy currents, electromagnetic devices, electromagnetic induction, inductive power transmission, proximity effects, Q measurement, wireless power transmission.**

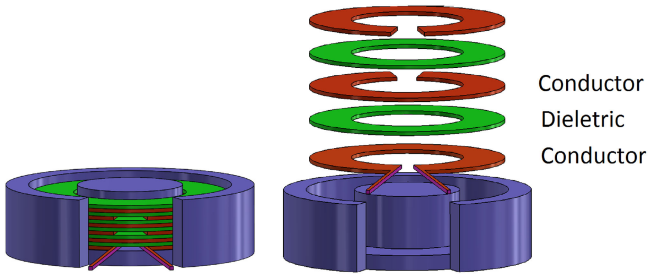

I. Introduction

WIRELESS power transfer (WPT) is of great interest for many applications including biomedical, automotive, and consumer hand-held electronics [1]–[4]. In many of these applications, a high-frequency magnetically-coupled resonant system is the most effective method of transmitting wireless power. The efficiency of such a system is limited by the quality factor and coupling factor of the resonant coils that generate the electromagnetic coupling [3], [5], [6]. As the range between the coils increases, the coupling factor decreases; therefore, im-

Manuscript received April 16, 2018; revised August 8, 2018; accepted September 22, 2018. Date of publication October 8, 2018; date of current version May 2, 2019. This work was supported by the National Science Foundation under Grant 1507773. Recommended for publication by Associate Editor M. Duffy. *(Corresponding author: Aaron L. F. Stein.)*

The authors are with the Thayer School of Engineering, Dartmouth College, Hanover, NH 03755 USA (e-mail:

conductors and a low loss dielectric to create a high-Q resonant coil [15]. This structure consists of alternating layers of C-shape foil conductors and dielectric rings placed in a ferrite core, and forms a parallel resonator in a single component. This integration of capacitance and inductance is similar to the integrated LC and LCT (inductor, capacitor, transformer) passive power components discussed in, for example, [16]–[18]. However, unlike the previous work, multi-layer self-resonant structures use the capacitance not only to implement the necessary capacitance, but also to make the conductors more efficient by equalizing current sharing between them. As a result, they not only provide a parts count savings through integration, but also provide a dramatic performance benefit. A structure similar to the multi-layer self-resonant structure is reported in [19], but insufficient detail is provided to assess its true capability. In particular, the inductance calculation assumes that all the flux is in the magnetic material, resulting in a major discrepancy in the calculated versus experimental inductance. No proximity effect losses are considered in the analysis and an appropriate measurement methodology for the Q value is not reported.

Thin foil layers are vital for the performance of the self-resonant structure, but can make prototyping difficult. To overcome this concern, we also propose a variation of the self-resonant structure that allows fabrication with more conventional methods and materials [20]. This modified structure uses high-loss but low-cost PCB substrates such as FR4 and polyimide to support thin conductor layers for easy handling without adversely affecting the quality factor of the resonance. The improved manufacturability of the modified structure presented here allowed us to successfully implement two high-Q 7 MHz resonant structures and demonstrate long-range and high-efficiency WPT.

A related type of self-resonant structure, proposed in [21], is a split-ring resonator (SRR), which is a pair of C-shaped conductors that forms a simple resonator. SRRs can be arrayed to create metamaterials with unusual and controllable electromagnetic properties, and have been proposed as a way to influence the coupling of resonant inductive WPT systems. However, although it can be shown that an ideal negative-permeability material could be used to enhance performance, the losses of practical SRRs limit the usefulness of this approach [22]. Whereas, an individual SRR comprises just two concentric C-shaped conductors, the self-resonant structure configures them in a stack rather than in an array, and uses many layers to achieve low losses, in conjunction with soft magnetic material shaping the field for lowest losses.

In this paper, we begin by describing the self-resonant structure and its loss mechanisms (Section II) [15], [20]. Next, we describe the modified self-resonant structure (Section III), which has similar performance as the self-resonant structure but is easier to prototype [20]. We then introduce new analysis of the structure's performance in a WPT system including: a lumped element model of two coupled self-resonant structures, the theoretical WPT efficiency, optimal operating conditions, and the impact of input resistance on WPT efficiency (Section IV). Finally, we present experimental results characterizing the structure [20], and new experiments demonstrating its performance in a WPT system (Section V).

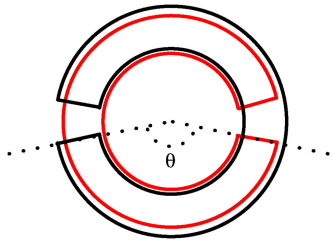

Fig. 2. In this figure, two overlapping C-shaped conductors forming one section are shown from a top–down perspective. Each section forms two capacitors C_{sh}, which are connected in series. The angle of overlap of one capacitor θ is indicated.

In addition to WPT applications, high-Q resonant structures are of interest as passive components for power converter applications. Design work and test results for similar structures used in resonant power conversion are discussed in [23] and [24].

II. Self-Resonant Structure

The self-resonant structure consists of a stack of M sections separated by a dielectric layer and placed inside a magnetic core. A section is two C-shaped foil layers separated by a low-loss dielectric (see Fig. 1). The C-shaped conductors within a section have opposite orientations, which results in two overlapping areas. The overlapping areas, depicted in Fig. 2, form two capacitors. As current flows through a section it passes through both capacitors, and creates an inductive current loop. This results in a parallel LC resonator in which the inductance L is equivalent to a single turn around the magnetic core and the capacitance is the series combination of two section-half capacitances C_{sh}. The capacitance can be expressed in terms of the angle of overlap of the layers in radians θ (shown in Fig. 2), the outer radius of the coil r_2, the inner radius r_1, the permittivity of the dielectric ϵ_d, and the dielectric thickness t_d as follows:

$$C_{\text{sh}} = \epsilon_d \left(\frac{\theta}{2\pi}\right)\left(\frac{\pi\left(r_2^2 - r_1^2\right)}{t_d}\right) = \frac{\epsilon_d \theta (r_2^2 - r_1^2)}{2t_d}. \quad (1)$$

In practical designs, the self-resonant structure is constructed from many sections that are separated from each other by a low-loss dielectric layer. Excluding the first layer, each section is inductively coupled so there are no terminations in the high-current path. The strong coupling effectively puts all of the sections in parallel. Each section has a capacitance $\frac{C_{\text{sh}}}{2}$, and there is additional capacitance between a section and the layers above and below it. Therefore, a structure with M sections has an equivalent capacitance C_{equiv} of $C_{\text{equiv}} = MC_{\text{sh}}$, and a resonant frequency $\frac{1}{\sqrt{LC_{\text{equiv}}}}$. A circuit model of a 3-section self-resonant structure is shown in Fig. 3. The strong coupling between sections forces each section to have approximately the same voltage, and therefore (for equal capacitances) the same current.

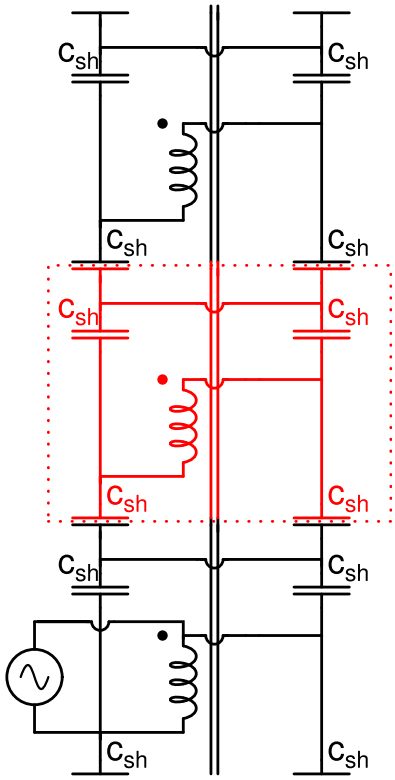

Fig. 3. Equivalent circuit model of a three-section self-resonant structure. The red section encompassed by a dotted square models a single section of the structure, and three of these sections are "stacked" to form the equivalent circuit model. The horizontal lines on the top and bottom of the diagram represents a conductive layer that would be used as part of a capacitor if additional sections were added.

A two-dimensional (2-D) illustrative simulation of a stack of five sections is shown in Fig. 4; Fig. 5 has a conceptual diagram of this configuration. The simulation shows that at the 0° position (left) current is flowing in the layers that are interrupted at 180° position. Over the next 180°, it gradually transfers to the opposing conductor layers, and then transfers back as we approach 360°. This scenario is illustrated in Fig. 5 where the end of each layer labeled I_L has the full layer current (I_L), and the other end (labeled 0), has zero current.

The self-resonant structure provides three main benefits over conventional resonant coils. First, capacitance ballasting forces equal current sharing between many thin foil layers. Easily obtained foil thicknesses are about an order of magnitude smaller than easily obtained Litz strand diameters; therefore, the self-resonant structure is able to mitigate skin and proximity effects in the megahertz frequency range, where Litz wire is ineffective. Second, the inductive coupling between sections means that, unlike conventional coils, there are no terminations in the main resonant-current path, and therefore minimal losses due to terminations. Finally, the self-resonant structure does not have plate losses associated with a conventional capacitor because the capacitance is integrated into the structure. For these reasons the self-resonant structure can achieve a much higher Q than conventional resonant coils.

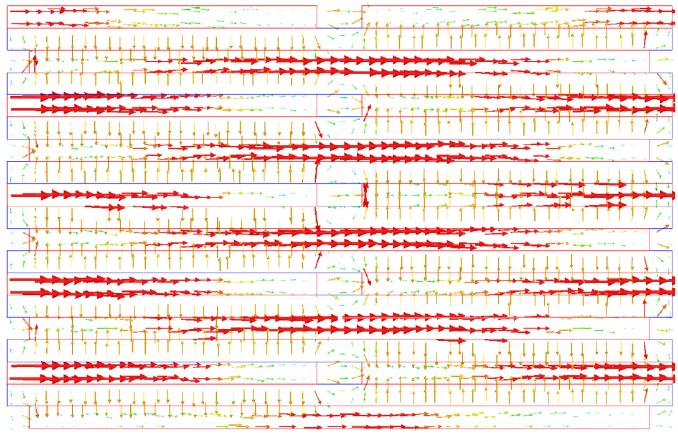

Fig. 4. 2-D illustrative simulation of conduction and displacement current flows in a stack of five sections. The cross section is an "unwrapped" circular section, such that the horizontal position in the figure corresponds to angular position 0° at the left and to 360° at the right. The conductor layers have primarily horizontal current flow (by conduction), while the dielectric layers have vertical displacement current flow. For clarity, the scales are different for displacement and conduction currents. The layer thicknesses are exaggerated in this illustration – our designs use layers that are much thinner in comparison to the perimeter.

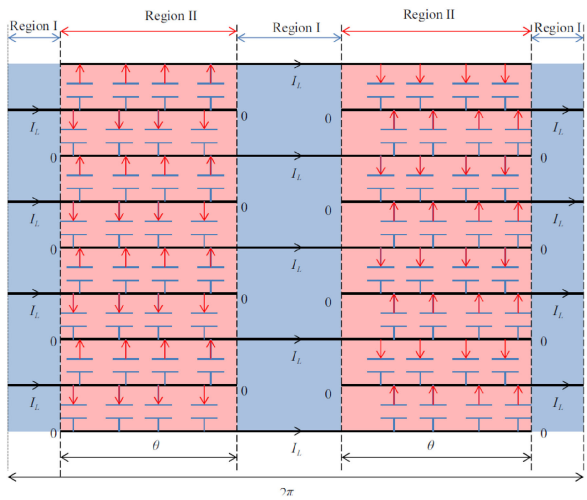

Fig. 5. Diagram corresponding to Fig. 4.

A. Loss Mechanisms

The performance of the self-resonant structure is measured by the quality factor of the device at resonance. The quality factor Q is

$$Q = \frac{\omega_o L}{R_{\text{total}}} \tag{2}$$

where R_{total} is the sum of three equivalent series resistances (ESR) that model winding loss, core loss, and dielectric loss. The ESR for each of these loss mechanisms is discussed in this section.

The focus of this paper is to extend the range and efficiency of WPT; therefore, the loss mechanisms are analyzed for a

single self-resonant structure, not two coupled structures. This approximates the behavior of a weakly coupled WPT system. In a strongly coupled system, the loss models must account for mutual resistances, and therefore would require a matrix of resistances.

1) Winding Loss: We first consider the resistive loss, defined for a non-resonant coil as $P_r = R_{\rm dc}\, I_{\rm rms}^2$, where $R_{\rm dc}$ is the dc resistance and $I_{\rm rms}$ is the rms current. It is not immediately clear what would be the analogy for dc resistance for a resonant coil, given that the capacitive coupling would block dc current. However, we can perform the analysis in terms of low-frequency ac resistance, R_{LF}, which, in a conventional winding, would be equal to the dc resistance.

As a starting point, we find the low-frequency resistance of a simple single-layer loop as

$$R_{\rm LF,loop} = \frac{2\pi\rho}{\ln\left(\frac{r_2}{r_1}\right)\cdot t_c} \tag{3}$$

where t_c is the thickness of the conductor, r_1 and r_2 are the inner and outer radii of the conductor, and ρ is the resistivity of the conductor material.

Comparing low-frequency resistance for a simple loop to that of a section comprising a pair of C-shapes, we find the low-frequency resistance is mildly reduced, based on the current being shared between two layers in the overlap region (see designated region II in Fig. 5). In this region, the current flow transfers from one C-shape to the adjacent ones over the distance of the overlap angle θ (shown in Fig. 2) and as a result, the current in a given layer, I_n, linearly increases or decreases as a function of angular position φ, ranging from zero to the full layer current I_L. This can be written as $I_n(\varphi) = I_L \cdot \frac{\varphi}{\theta}$ or $I_n(\varphi) = I_L \cdot \left(1 - \frac{\varphi}{\theta}\right)$, in region II. Integrating the square of this current with respect to angle, we find that the power loss in the overlapping region of each C-shape is 1/3 of what it would be with constant current, for a total power loss in region II of a section (comprising two C-shapes) equal to 2/3 of the power loss that would result from the current flowing in a simple single layer.

Given that the current must flow a total angular distance 2θ in the overlap region (region II) and a total angular distance $2(\pi-\theta)$ in region I (where there is no overlap), we can find the total resistance around the loop in one section (a pair of C-shapes) by using $R_{\rm LF,loop}$ or 2/3 or $R_{\rm LF,loop}$ for the appropriate fraction of the full 2π radians in the loop as follows:

$$R_{{\rm LF},M} = R_{\rm LF,loop}\left(\frac{2\,(\pi-\theta)+\frac{2}{3}2\theta}{2\pi}\right). \tag{4}$$

Simplifying this, we see that $R_{\rm LF}$ is reduced by a factor $k_1 = 1 - \frac{\theta}{3\pi}$. The result shows that for the full range of possible overlap angles from zero to 180°, the low-frequency resistance varies between the full resistance of a simple loop (for small overlap angles) and 2/3 of that value (for maximum overlap).

If we assume that the current shares equally between M sections, the effective resistance seen by the total rms current $I_{\rm rms}$ is $R_{\rm LF,loop}\cdot k_1/M$, such that

$$P_r = I_{\rm rms}^2 \cdot R_{\rm LF,loop}\cdot\frac{k_1}{M}. \tag{5}$$

Next we consider eddy-current loss (proximity effect), which is caused by a time varying magnetic field in the winding. A typical proximity effect analysis assuming a 1-D field is created by a magnetic core with infinite permeability and placed directly adjacent to both edges of the windings, such that it provides a magnetic flux path with no reluctance. In practice, there is a gap between the magnetic core and the winding. Furthermore, the permeability of the high frequency magnetic material is not large enough to be accurately modeled as infinite. Compared to the idealized case, these practical consideration weaken the magnetic field and prevent the magnetic field lines from being perfectly parallel to the foil layers. Our analysis first finds an expression for the proximity-effect loss assuming a 1-D field as described earlier, and then modifies this expression to take into account 2-D fields created by practical winding placement and core permeability.

The ac resistance factor assuming a 1-D field F_{1dr} is derived in Appendix A, and is as follows:

$$F_{1dr} = \frac{R_{ac}}{R_{lf}} = 1 + \frac{M^2}{9}\left(\frac{t_c}{\delta}\right)^4\cdot\frac{k_2}{k_1} \tag{6}$$

where t_c is the thickness of the conductor, δ is the skin depth, and k_2 is $1+\frac{\theta}{\pi}$. This is a standard expression for an ac resistance factor in a multilayer structure, but modified by the factor $\frac{k_2}{k_1}$.

Next, we consider the impact of a 2-D field created by practical winding placement and core permeability. When the magnetic field lines are not parallel to the foil layers, there is increased winding loss due to horizontal current crowding. This is modeled with a current crowding factor $F_{\rm cc}$, which is extracted from a finite element analysis (FEA) as described in Appendix B-B. In the idealized case $F_{\rm cc}$ is 1, and it increases in practical scenarios. Furthermore, the winding placement and core permeability weaken the magnetic field which reduces the proximity effect. The impact of field weakening on the winding resistance is modeled by a field weakening factor $F_{\rm fw}$, which is extracted from an FEA described in Appendix B-A. In the idealized case, $F_{\rm fw}$ is 1, and it decreases in practical scenarios. The ac resistance factor including current crowding and field weakening is

$$F_r = F_{\rm cc} + \frac{F_{\rm fw}M^2}{9}\left(\frac{t_c}{\delta}\right)^4\frac{k_2}{k_1}. \tag{7}$$

In summary, the winding loss model is

$$R_{\rm wind} \approx \frac{2\pi\rho}{\ln(\frac{r_2}{r_1})t_c M}\left[k_1 F_{\rm cc} + \frac{F_{\rm fw}M^2}{9}\left(\frac{t_c}{\delta}\right)^4 k_2\right] \tag{8}$$

where $k_1 = 1-\frac{\theta}{3\pi}$ and $k_2 = 1+\frac{\theta}{\pi}$.

2) Magnetic Core Loss: The appropriate core loss model is dependent on the flux density in the magnetic core [25]. If the flux density is relatively small, then the core loss should be found from a complex permeability loss model, and if the flux density is relatively large, then the core loss should be found using the Steinmetz equation. In many WPT applications, including our prototyping work, the relatively large gap causes the flux density in the core to be relatively low; therefore, in this section an expression for the core loss is derived from the complex permeability loss model.

Incorporating the complex permeability of the core in a reluctance model results in an expression for a complex valued single-turn inductance as follows:

$$L^* = \frac{1}{\frac{\ell_{\text{eh}}}{A_e \mu_0 (\mu' - j\mu'')} + \mathscr{R}_a} \tag{9}$$

where ℓ_{eh} is the effective length of the core half (half the effective length of a full pot core), A_e is the effective area of the core, $\mathscr{R}_a$ is the reluctance of the air gap, and $\mu' - j\mu''$ is the relative permeability of the magnetic core. The ESR that models core loss is a function of the angular frequency ω and is given by

$$R_{\text{core}} = \Re\left[j\omega L^*\right] = \frac{\omega \frac{\ell_{eh}}{\mu_0 A_e} \mu''}{\left(\frac{\ell_{eh}}{\mu_0 A_e} + \mathscr{R}_a \mu'\right)^2 + \left(\mathscr{R}_a \mu''\right)^2}. \tag{10}$$

To simplify this expression in order to obtain design insight, we first neglect the $(\mathscr{R}_a \mu'')^2$, because, for an effective core, it is much smaller than $(\mathscr{R}_a \mu')^2$. Although the $\frac{\ell_{\text{eh}}}{\mu_0 A_e}$ term could be significant, in our prototyping work we found that the $\mathscr{R}_a \mu'$ term dominates. In this case, the ESR arising from core loss is approximately proportional to

$$R_{\text{core}} \tilde{\propto} \frac{1}{\mu' Q_{\text{material}}} \tag{11}$$

where the quality factor of the material Q_{material} is $\frac{\mu'}{\mu''}$. Therefore, we chose a material that has both a large Q_{material} and a large real component of magnetic permeability at the resonant frequency of the structure. However, (11) does not always hold. For example, if the magnetic core was very thin, $\frac{\ell_{\text{eh}}}{\mu_0 A_e}$ could be the dominant term, and in this case $R_{\text{core}} \tilde{\propto} \mu''$.

3) Dielectric Loss: The losses created by the capacitance C_{equiv} of the structure are due to the dielectric material, and can be modeled with an ESR that is given by

$$R_{\text{dieletrcic}} = \frac{D_d}{C_{\text{equiv}} \omega} \tag{12}$$

where D_d is the dissipation factor of the dielectric. To reduce the dielectric loss, a material with a small dissipation factor such as polytetrafluoroethylene (PTFE) or polypropylene should be used. The dielectric loss ESR is smaller than the ESR of an external capacitor, because the capacitor ESR would also include resistive and eddy-current losses in the conductors.

B. Coil Optimization

Designing an effective self-resonant structure requires a balance of conductor thickness, dielectric thickness, and overlap angle. For example, for a given number of sections, if the conductor is too thick, the proximity-effect losses will be high, whereas if the conductor is too thin, the low-frequency resistance will be large. Similarly, an optimal number of sections exists for a given conductor thickness. If too many sections are used, the proximity-effect losses will once again be high, and if too few sections are used the conductor resistance will be high. In the work done in [15], we derived expressions for: the optimal conductor thickness given a number of sections constraint, and the optimal number of sections given a conductor thickness constraint. In that analysis, we showed that if the optimal conductor thickness is used, the optimal overlap angle is the largest feasible angle. This choice also allows the use of thicker dielectric which is easier to work with, and is used in all of our designs. In our prototyping work, we chose to use readily available commercial materials rather than optimal thicknesses. A contour plot of the design space, such as Fig. 6, is useful in this case to obtain an overview of the design space and to consider practical but sub-optimal designs. The impacts of various design choices on our prototypes are discussed in Section V-A.

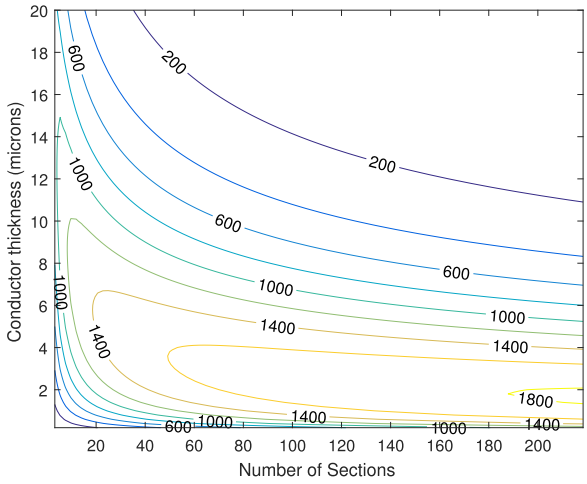

Fig. 6. Contour lines of the theoretical quality factor of the self-resonant structure at 7 MHz as a function of the conductor thickness and the number of sections for a 6.6 cm pot described in Section V. In this figure the overlap angle is 170°, and both the field weakening factor and current crowding factor are 1.

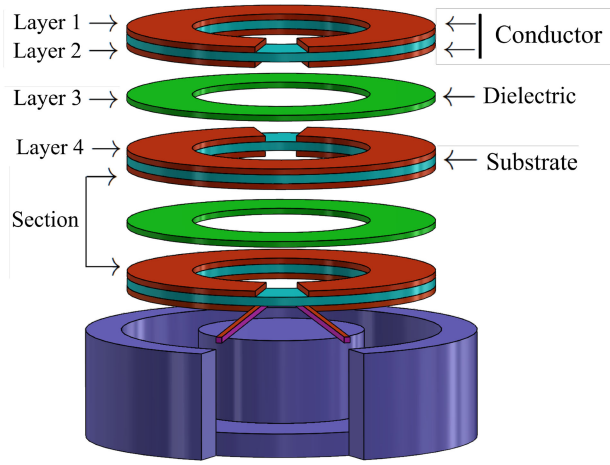

Fig. 7. Layers of a two-section modified self-resonant structure.

III. Modified Self-Resonant Structure

The self-resonant structure requires thin foil layers in order to effectively mitigate skin and proximity effect; however, these thin foil layer can be difficult to handle. To overcome this challenge, we propose the modified self resonant structure which is depicted in Fig. 7. This structure allows the use of low-cost but low-performance PCB substrates such as FR4 or polyimide to support thin conductive layers without significantly affecting

the Q of the structure. If the structure shown in Fig. 1 was built using such substrates, excessive dielectric losses would result. But in the modified structure, any two conductor layers that are separated by a high-loss substrate are oriented with their gaps aligned. For example, in Fig. 7, the top layer of copper (layer 1) is separated from the second layer of copper (layer 2) by a high-loss substrate, and are both oriented such that the gap is coming out of the page. A capacitance C_{sub} is formed between these two layers; however, the orientation ensures that no strong electric field is generated between the layers. The voltage induced in C_{sub} is only due to the leakage magnetic flux, which is a small fraction of the overall magnetic flux. This allows the use of the high-loss substrate without significantly affecting the quality factor. A calculation of the loss in the substrate in Appendix C shows that, for our prototyping work, the loss is four orders of magnitude smaller than the other computed losses. The other loss mechanisms are the same for modified self-resonant structure and the self-resonant structure (Section II-A); therefore, the modified self-resonant structure can achieve similar performance as the self-resonant structure while supporting the thin foil layers on a low-cost substrate.

The modified structure has an equivalent capacitance $C_{\text{equiv}} = \frac{m C_{\text{sh}}}{2}$, which is half the capacitance of the original self-resonant structure, for a given dielectric thickness and numbers of sections. Therefore, for a given geometry, the modified structure requires either twice as many sections, or half the dielectric thickness in order to maintain the same resonant frequency. An equivalent circuit model of the modified structure is shown in Fig. 8.

The substrate material does not impact the equivalent capacitance C_{equiv} or the quality factor of the modified self-resonant structure, so it can be selected based on considerations such as: ease of handling, the overall compactness of the complete structure, cost, and manufacturability. Low-cost substrates such as FR4 and polyimide are commonly laminated with copper and etched using standard PCB processes, which makes them excellent candidates for constructing the substrate layer. However, any insulating and non-magnetic material could be used to form the substrate layer, as the dielectric properties do not impact the Q of the modified structure.

It should be noted that, although the substrate layers do not impact the Q, the properties of the dielectric layers are critical to the performance of the modified structure. The dissipation factor of the dielectric layers has a similar impact on the Q of the self-resonant structure and the modified self-resonant structure; therefore, low-loss dielectric materials (e.g., PTFE or polypropylene) should be used for the dielectric layers of the modified structure.

IV. Wireless Power Transfer

The maximum achievable efficiency η_{max} between two coils of a WPT system is dependent on the quality factor Q_1 of the send coil, the quality factor Q_2 of the receive coil, and the magnetic coupling coefficient k. The theoretical maximum efficiency can be found from the optimal loss fraction presented

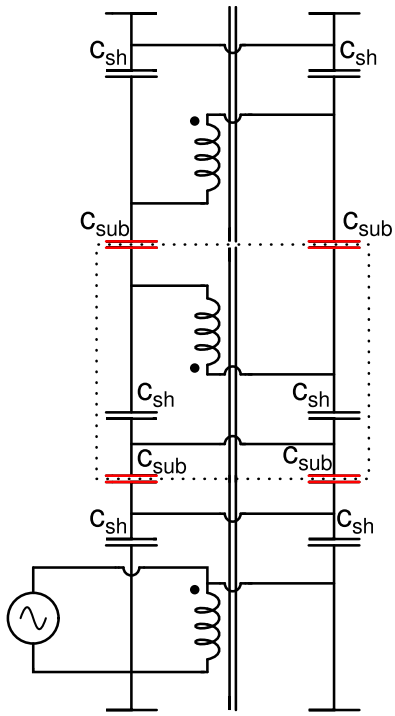

Fig. 8. Equivalent circuit model of a three-section modified self-resonant structure. The dashed line encompasses a single section, and three of them are "stacked" on top of each other with alternating orientation. This orientation ensure that the capacitors formed through a high-loss substrate (shown in red) are not excited by the resonance. The horizontal lines on the top and bottom of the diagram represents a conductive layer that would be used to form a capacitor if additional sections were added.

in the work done in [5] and is given by

$$\eta_{\text{max}} = \frac{Q_1 Q_2 k^2}{\left(1 + \sqrt{1 + Q_1 Q_2 k^2}\right)^2}. \tag{13}$$

In practice, loss mechanisms not accounted for by the Q of the structure, variations from the optimal load, and impedance matching all can cause the efficiency of WPT to be less than the theoretical maximum. In this section, we present a lumped element model of two coupled self-resonant structures in order to provide a more accurate estimate of the system efficiency, provide a methodology for deriving the optimal load resistance and drive frequency, and illuminate the impact of various loss mechanisms on the overall wireless efficiency. This analysis applies to both the modified self-resonant structure and the self-resonant structure.

A lumped element model of the two coupled self-resonant structures is shown in Fig. 9. A single self-resonant structure is modeled as the parallel combination of an equivalent inductor, capacitor, and resistor, C_1, R_1, and L_{s1} for the send structure and C_2, R_2, and L_{s2} for the receive structure. We define Z_1 and Z_2 as the parallel combinations of C_1, R_1, and L_{s1}, and of C_2, R_2, and L_{s2}, respectively. We also define the input voltage as V_{in}, the output voltage as V_o, and the voltage on the send structure resonator as V_1 (see Fig. 9). The magnetic coupling between the structures is modeled using a π transformer model. The

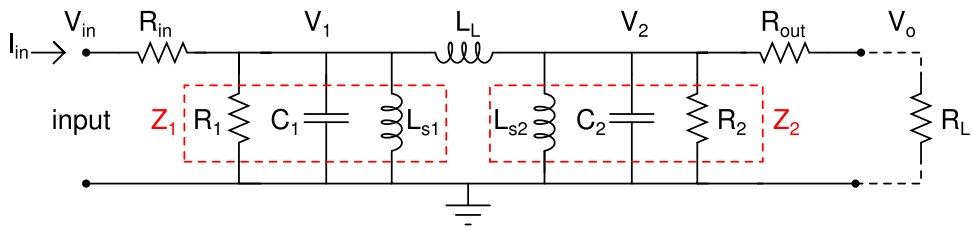

Fig. 9. Lumped element model of two self-resonant structures magnetically coupled together for WPT. A load resistor R_L is shown, but is not inherent to the structure.

connection to the self-resonant structure is a split ring with foil leads on it, which has a relatively high resistance because it does not benefit from the many parallel thin layers associated with the structure. The connection to the send structure is modeled with a resistor R_{in}, and the connection to the receive structure is modeled with a resistor R_{out}. The load is a resistor R_L connected to the receive structure.

The efficiency η of WPT between two modified self-resonant structures is found from the loss fractions associated with the individual loss mechanisms

$$\eta = \frac{1}{1+\lambda} = \frac{1}{1+(\lambda_1+\lambda_2+\lambda_{R_{\text{in}}}+\lambda_{R_{\text{out}}})} \tag{14}$$

where λ_1, λ_2, $\lambda_{R_{\text{in}}}$, and $\lambda_{R_{\text{out}}}$ are the loss fractions associated with R_1, R_2, R_{in}, and R_{out}, respectively. The loss fraction for the receive structure λ_2 is the ratio of the power dissipated in R_2 to the power dissipated in R_L, and is

$$\lambda_2 = \frac{\frac{V_{2_{\text{RMS}}}^2}{R_2}}{\frac{V_{o_{\text{RMS}}}^2}{R_L}} = \frac{R_L^2}{R_2\,(R_L+R_{\text{out}})}. \tag{15}$$

The loss fraction for the send coil is $\lambda_1 = \frac{V_{1_{\text{RMS}}}^2}{R_1}\frac{R_L}{V_{o_{\text{RMS}}}^2}$. We define a factor $F_{1o} = \frac{V_1}{V_o}$, that is the ratio of V_1 to V_o, where

$$F_{1o} = \left(\frac{j\omega L_L}{Z_2} + \frac{j\omega L_L}{R_L} + 1\right)\frac{R_L+R_{\text{out}}}{R_L} \tag{16}$$

therefore,

$$\lambda_1 = \frac{R_L}{R_1}||F_{1o}||^2. \tag{17}$$

The loss fraction for the input resistance is $\lambda_{R_{\text{in}}} = \frac{I_{\text{in}_{\text{RMS}}}^2 R_{\text{in}} R_L}{V_{o_{\text{RMS}}}^2}$. The input current I_{in} expressed in terms of V_o is $I_{\text{in}} = V_o\left(\frac{F_{1o}}{Z_1} + \frac{R_{\text{out}}+R_L}{R_L Z_2} + \frac{1}{R_L}\right)$. Therefore, $\lambda_{R_{\text{in}}}$ can be simplified to

$$\lambda_{R_{\text{in}}} = \frac{I_{\text{in}_{\text{RMS}}}^2 R_{\text{in}}}{\frac{V_{o_{\text{RMS}}}^2}{R_L}} = R_{\text{in}} R_L \left|\left|\frac{F_{1o}}{Z_1} + \frac{R_{\text{out}}+R_L}{R_L Z_2} + \frac{1}{R_L}\right|\right|^2. \tag{18}$$

Finally, the lost fraction for the output resistance is $\lambda_{R_{\text{out}}} = \frac{R_{\text{out}}}{R_L}$.

The loss faction for the entire system λ is

$$\begin{aligned}\lambda &= \lambda_1 + \lambda_2 + \lambda_{R_{\text{in}}} + \lambda_{R_{\text{out}}} \\ &= \frac{R_L||F_{1o}||^2}{R_1} + \frac{R_L^2}{R_2\,(R_L+R_{\text{out}})} \\ &\quad + R_{\text{in}} R_L \left|\left|\frac{F_{1o}}{Z_1} + \frac{R_{\text{out}}+R_L}{R_L Z_2} + \frac{1}{R_L}\right|\right|^2 + \frac{R_{\text{out}} R_L}{R_L^2}.\end{aligned} \tag{19}$$

The optimal load resistance and drive frequency can be found by minimizing (19).

The resistance of the first layer, which is modeled by R_{in} and R_{out}, will be much higher than the ESR of a well designed self-resonant structure. However, at practical WPT transmission distances the current in the first layer is substantially less than the current shared by the many layers of the self-resonant structure; therefore, the first layer typically has only a small impact on the system efficiency, so the efficiency of a system utilizing these structures can approach η_{max}. The impact of R_{in} and R_{out} on the WPT efficiency of our prototyping work is discussed in Section V-C.

V. Modified Self-Resonant Structure Experimental Results

We constructed and tested a pair of modified self-resonant structures with resonant frequencies near the industrial, scientific, and medical radio (ISM) band of 6.78 MHz. The modified structure was used for prototyping because it provided a convenient way to handle thin conductive layers. Section V-A details the implementation of these structures, Section V-B presents experimental impedance measurements, and Section V-C shows experimental WPT efficiency data.

A. Implementation of the Modified Self-Resonant Structure

The modified self-resonant structure comprises three main components. First, a pot core with a diameter of 6.6 cm was made from Fair-Rite's 67 material, chosen for its relatively high permeability (40 μ_0) and high Q_{material} (712) at 6.78 MHz. Next, the conductive layers of the structure were created using 6 μm copper that, for ease of handling, was laminated on both sides of a 25 μm polyimide substrate and patterned into C-shapes using standard PCB fabrication processes. Finally, 50.8 μm thick PTFE film was cut with a die cutter to form the low-loss dielectric layers. A picture of one of the modified self-resonant

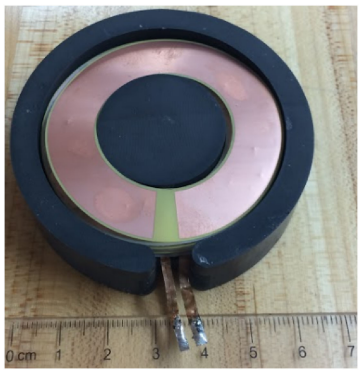

Fig. 10. Picture of the modified self-resonant structure that was used for experimental results.

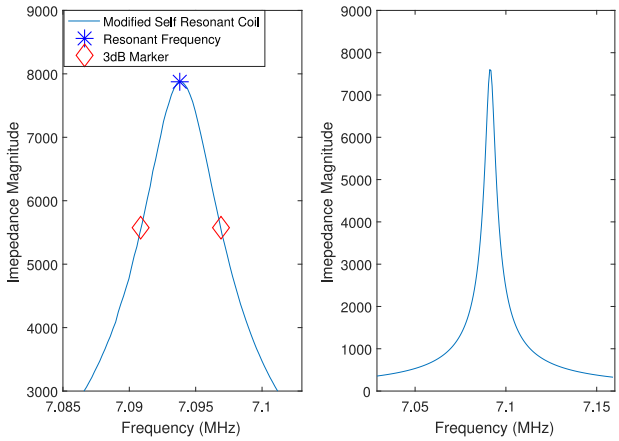

Fig. 11. Agilent 4294A impedance analyzer was used to measure the impedance magnitude of the modified self-resonant structure around its resonant frequency. The impedance magnitude is shown for two different frequency ranges to illustrate the high-Q nature of the resonance. The experimental measured quality factor of the modified self-resonant structure is 1183.

TABLE I
EXPERIMENTAL EFFICIENCY, LOAD RESISTANCE, AND MATCHING NETWORK PARAMETERS REPORTED AT VARIOUS TRANSMISSION DISTANCES FOR THE EXPERIMENTAL WPT SYSTEM

Parameter	Description	Value
d	Structure diameter	6.6 cm
M	Number of sections	48
	Core window height	9.2 mm
	Structure height	16 mm
r_2	Coil outer radius	26.25 mm
r_1	Coil inner radius	14.85 mm
t_c	Conductor thickness	6 μm
t_s	Substrate thickness	25.4 μm
	Winding stack height	5.5 mm
θ	Overlap angle	170°
δ	Skin depth	24.5 μm
ρ	Conductor resistivity	16.8 nΩ-m
F_{fw}	Field weakening factor	0.80
F_{cc}	Current crowding factor	1.74
R_{wind}	Winding ESR	1.68 mΩ
L	Structure inductance	137 nH
μ'	Core relative permeability	48.1
μ''	Imaginary relative permeability	0.0781
ℓ_{eh}	Effective length of core half	37.5 mm
A_e	Effective core area	717 mm^2
$\mathscr{R}_a$	Reluctance of air path	6.23 $\frac{\text{MA}}{\text{Wb}}$
R_{core}	Core ESR	1.19 mΩ
C_{equiv}	Structure capacitance	3.67 nF
t_d	Dielectric thickness	25.4 μm
ϵ_d	Dielectric permittivity	$2.2\epsilon_o$
ϵ_s	Substrate permittivity	$3.4\epsilon_o$
D_d	Dielectric dissipation factor	2×10^{-4}
D_s	Substrate dissipation factor	.0018
$R_{dieletric}$	Dielectric ESR	1.22 mΩ
R_{sub}	Substrate ESR	99.5 nΩ

structures is shown in Fig. 10, and system parameter values are catalogued in Table I.

The copper thickness, dielectric thickness, and number of sections were chosen in order to maximize the quality factor of the structure given commercially available materials and practical construction constraints. The dielectric thickness (50.8 μm) was chosen so that the dielectric material could be easily handled without wrinkling. The core geometry was fixed, so, given an overlap angle of 170°, the dielectric thickness determined the minimum number of sections required in order to achieve the desired resonant frequency ($M = 48$). The optimal conductor thickness for 48 sections is 4.7 μm, but we chose a polyimide substrate laminated with 6 μm copper because it was commercially available. Given the chosen conductor thickness and number of section, the optimal overlap angle θ is very small, but reducing the overlap angle would require a thinner and more difficult to handle dielectric in order to maintain the resonant frequency.

For this implementation, the analysis in Section II-A estimates the total ESR to be 4.10 mΩ. An FEA is used to estimate the field weakening factor F_{fw} of 0.80, and the current crowding factor F_{cc} of 1.74, which results in a predicted winding resistance of 1.68 mΩ. Measurements of FairRite 67 material in our pot core shape found the relative permeability to be $48.1 - j0.0781$, which results in a core loss ESR of 1.19 mΩ. The maximum flux density in our experiments was calculated to be 0.846 mT. At this flux density, the estimated core loss using a Steinmetz model is 2.39 mW, and the core loss using the complex permeability is 30.9 mW. Therefore, based on the work done in [25], the complex permeability model of the core loss in Section II-A2 is appropriate for our application. Finally, for the dissipation factor of the PTFE dielectric, we use the commonly reported value $D_d = 2 \times 10^{-4}$, resulting in an ESR representing dielectric loss of 1.22 mΩ. Because reported data is scant and precise measurements of such a low dissipation factor is difficult, there is significant uncertainty in the dissipation factor. However, the dielectric loss is only a small fraction of the overall loss, so deviations from our estimated dissipation factor would not drastically change the estimated quality factor. From (2) and the inductance, which is 137 nH, we calculate an expected quality factor of 1490.

TABLE II
SUMMARY OF EXPERIMENTAL RESULTS FOR TWO MODIFIED SELF-RESONANT STRUCTURES

Parameter	Description	Structure 1 Value	Structure 2 Value
f_o	Resonant frequency	$f_{o_1} = 6.99$ MHz	$f_{o_2} = 7.09$ MHz
Q	Quality factor	$Q_1 = 1133$ or 1225	$Q_2 = 1183$ or 1290
Q_d	Figure of merit (FOM)	169 or 185	179 or 195
	FOM percent increase	504% or 561%	539% or 596%

Two methods were used to calculate the quality factor of the structures and both results are reported in this table (bandwidth method, Z_{pk} method).

B. Experimental Performance of the Modified Self-Resonant Structure

The experimental quality factor of the modified self-resonant structure was determined using two methods in order to verify the measurements. First, the quality factor was found to be 1183 using the ratio of the resonant frequency to the 3 dB bandwidth extracted from Fig. 11, which is the magnitude of the device impedance versus frequency measured with an Agilent 4294A impedance analyzer. Next, the quality factor was also calculated from the simulated structure inductance, the experimental resonant frequency, and the experimental magnitude of the maximum impedance Z_{pk} to compute $Q = \frac{Z_{pk}}{\omega_o L} = 1290$. There is only an 8.6% difference between the quality factor calculated with each method, which validates our measurement methodologies.

The quality factor measurements have a 13.4% error and 20.6% error between the theoretical and experimental quality factor, which suggests good agreement with the analysis presented in Section II-A. The disagreement between the experimental result and the theoretical findings are likely caused by three factors. First, it is challenging to accurately measure the Q of a high-Q resonator, as shown by the 8.6% error between the two methods of measuring Q presented earlier. Second, imperfections in the construction process will cause conductive layers to not be perfectly flat and parallel, which results in the measured quality factor to be less than the theory predicts. Third, uncertainty in the material properties (e.g., D_d) creates some uncertainty in the theoretical Q.

The Q_d of the modified resonant structure is at least 179 cm^{-1}, which represents more than a 6x improvement over largest Q_d we found in the literature ($Q_d = 28$). An additional structure was constructed according to the same design to complete a pair for WPT experiments reported in Section V-C. The experimental results for both structures are summarized in Table II.

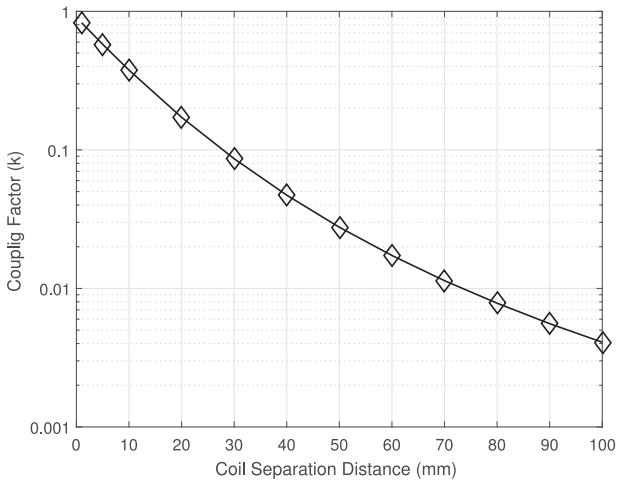

Fig. 12. Finite element analysis is used to find the coupling coefficient (k) as a function of the distance between the resonant coils.

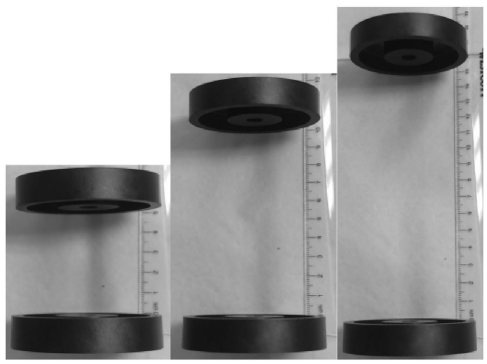

Fig. 13. Picture of the magnetic cores at a separation distances of (a) 50 mm, (b) 100 mm, and (c) 150 mm illustrates the relative size of the coil to the range of WPT discussed in this work.

C. Wireless Power Transfer Efficiency Utilizing the Modified Self-Resonant Structure

We tested WPT between the two structures in Table II. Structure 1 was the send structure and Structure 2 was the receive structure. The experimental results are compared to the theoretical maximum efficiency and the efficiency estimated by the lumped element model (described in Section IV). In this section, we describe how parameters were extracted for the theoretical maximum efficiency and lumped element model, detail the experimental setup, and present experimental WPT efficiency data.

1) Theoretical WPT Efficiency: The theoretical maximum efficiency of WPT is determined by both the quality factor of the self-resonant structures and the magnetic coupling factor. An FEA of the magnetic core shows that the coupling factor ranges from 0.875 to 0.0014 as the transmission distance increases from 1 to 150 mm (see Fig. 12). Fig. 13 illustrates the relationship between core size and transmission distance.

The theoretical maximum efficiency is plotted as a function of distances in Fig. 15. It was calculated using the quality factors

TABLE III
ESTIMATED ELEMENT VALUES FOR THE LUMPED ELEMENT MODEL PRESENTED IN FIG. 9

Name	Value	Name	Value
R_1	6.7 kΩ	R_2	7.2 kΩ
C_1	3.76 nF	C_2	3.65 nF
R_{in}, R_{out}	14.5 mΩ	R_L	0.010 - 2 kΩ
L_s	667 - 139 nH	L_L	0.4 - 40 μH

R_L, L_L, and L_s change with transmission distance, and are therefore reported as a range. These values are specific to the modified self-resonant structures presented in this section.

of the self-resonant structure reported in Table II, the coupling factor shown in Fig. 12 and (13).

The lumped element model from Section IV provides optimal operating conditions and a more accurate estimate of efficiency. The values of the elements in the model are obtained from theoretical analysis and experimental data from the individual coils. The inductances in the model are extracted from a magnetostatic FEA tool called Finite Element Method Magnetics. The FEA is executed using an axis-symmetric model of the magnetic core and winding. The winding is modeled as a single turn around the magnetic core that encompasses the entire area of the stack of copper and dielectric. The structure achieves nearly uniform current density, so the proposed simulation accurately models the structure without modeling the individual layers, which would require a very fine mesh and significantly lengthen the simulation time. The inductances L_{s1}, L_{s2}, and L_L are a function of transmission distance, and are extracted from a simulation using two different excitation configurations of two separated pot cores. The capacitances C_1 and C_2 are calculated from the measured resonant frequencies of their respective structures, and the inductance L_o extracted from a magnetostatic FEA of a single open faced pot core. The resistances (R_1, R_2) are calculated from the quality factor as $R = Q2\pi f_o L_o$. Finally, the input resistance R_{in} is the ac resistance of the first layer including the attached leads, and is calculated based on the mean current path length and the cross-sectional area (width times skin-depth). The impedance values are listed in Table III, and the resulting WPT efficiency is shown in Fig. 15.

The lumped element model predicts the efficiency to be within 1% of the theoretical maximum over the range of 1–100 mm. The small deviation between the theoretical maximum efficiency and the efficiency predicted by the lumped element model is mostly due to the resistance of the first layer of the send and receive structure, R_{in} and R_{out}. Although the first layer resistance is nearly four times the ESR of the self-resonant coil, it typically does not significantly impact the efficiency of the structure because it carries much less current. The loss fractions $\lambda_{R_{\text{in}}}$ and $\lambda_{R_{\text{out}}}$ are more than an order of magnitude smaller than λ_{R_1} and λ_{R_2} when the transmission distance is larger than 20 mm (see Fig. 14).

2) WPT Experimental Results: The experimental efficiency was found by exciting the send coil with a 50-Ω RF amplifier (Tomco BT00500). An impedance matching network was used to interface the WPT system and the amplifier. The values of

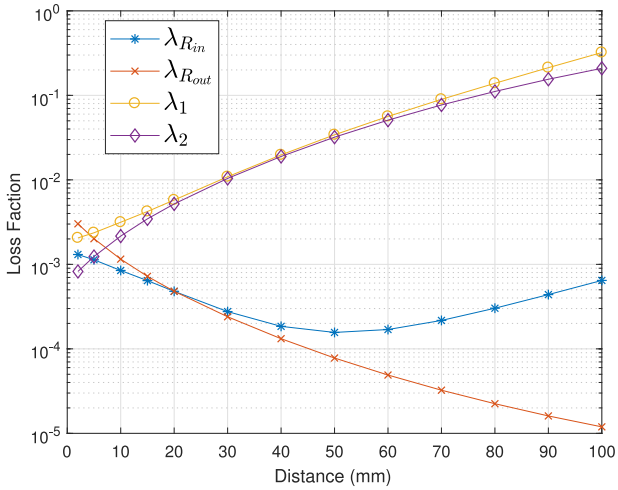

Fig. 14. Loss fraction of the input resistance $\lambda_{R_{\text{in}}}$, output resistance R_{out}, the send structure λ_1, and the receive structure λ_2 are plotted versus WPT range. Despite the relatively large resistances of R_{in} and R_{out}, they have an extremely small loss fraction, and therefore do not significantly impact the efficiency of WPT.

the matching network (see Table IV) were calculated so that the impedance of the WPT system was approximately 50 Ω. The input current (measured with a Tektronix P6022 current probe) and voltage before the matching network were acquired with a digital oscilloscope, and the average of instantaneous power wave was calculated on the oscilloscope. The theoretical power loss from the matching network was less than 1% of the total power; therefore the precision of this loss calculation does not significantly impact the overall efficiency. The output power was calculated from the RMS output voltage and the load resistance value. The load resistors used were TE 3522 Series resistors, and to ensure these resistors provided a resistive load at 7 MHz, we measured their high-frequency impedance. The experimental efficiency measurements were 94.0% at 50 mm, 80.6% at 77 mm, and 70.1% at 89 mm (see Table IV). The output power for the experiments ranged between 1 and 1.5 W. A relatively low-power level was chosen, so that neither nonlinear core loss nor thermal fluctuations impacted the WPT performance of the structure. The impact of high-power levels on the performance of the self-resonant structure is explored in the work done in [26], and constraints on the maximum power handling of the structure are discussed in [26] and [27].

The theoretical maximum efficiency and lumped element model efficiency are compared to experimental efficiency results in Fig. 15. The error between the experimental data efficiencies and the lumped element model efficiencies is less than 4%. This demonstrates good agreement between the experimental data and the theory presented in Sections II-A and IV.

In order to gauge the performance benefit of the modified self-resonant structure, the self-resonant structure efficiency is compared to the current state-of-the-art coil designs in Fig. 15. Since coupling factors of the state-of-the-art designs were not available as a function of distance, we calculate performance based on the same coupling factor as in our structure, but with a quality factor of 185. This quality factor is calculated by

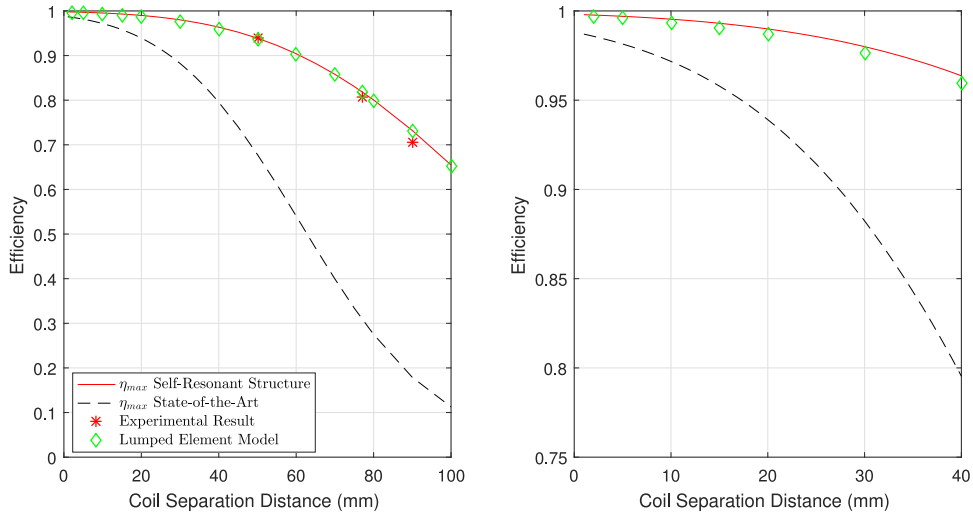

Fig. 15. Theoretical maximum WPT efficiency versus distance is shown for both the modified self-resonant structure, and the current state-of-the-art coil design (Q = 185). The plot on the right is a zoomed version of the plot on the left to clearly show the short-range performance. Both the experimental efficiency and the efficiency predicted from the lumped element model are shown for the self-resonant structure, and demonstrate agreement between the theoretical analysis and experimental data.

TABLE IV
EXPERIMENTAL EFFICIENCY, LOAD RESISTANCE, AND L MATCHING NETWORK PARAMETERS REPORTED AT VARIOUS TRANSMISSION DISTANCES FOR THE EXPERIMENTAL WPT SYSTEM

Distance	Load Resistance	Inductor Value	Capacitor Value	Efficiency
50 mm	100 ohm	3.7 μH	120 pF	94.0 %
77 mm	560 ohm	3.7 μH	None	80.6 %
89 mm	1120 ohm	5.2 μH	None	70.1 %

multiplying the state-of-the-art Q_d by the diameter of the core. The state-of-the-art WPT efficiency plotted is the theoretical maximum efficiency in order to provide the most optimistic baseline for comparison.

The modified self-resonant structure improves WPT efficiency over state-of-the-art coil designs for any distance between the coils that we have explored. For example, if the coils are 50 mm apart, experimental data shows that the modified self-resonant structure can achieve 94% efficiency, while the current state-of-the-art coil technology can achieve 67%. At longer distances, the difference is even more dramatic. At a distance of 90 mm, the state-of-the-art coil design can only achieve an efficiency of 18%, while experimental data using the modified self-resonant structures shows that they can achieve an efficiency of 70%.

VI. CONCLUSION

In this paper, we present a new high-Q resonant structure to increase the range and efficiency of WPT. It allows the effective use of very thin foil conductors for very low eddy-current losses, while also integrating resonant capacitance in order to avoid the need for high-current connections to external capacitors. The coil can be made from inexpensive materials with simple fabrication: no vias are required and every layer except the first one requires no soldered connections.

The thin foil layers can be difficult to handle without damaging, so we also propose a modified self-resonant structure that allows conductive layers to be laminated onto low-cost but high-loss PCB substrates such as FR4 or polyimide. We show that by orienting the layers on the two sides of the high-loss substrate in the same direction, we avoid exciting the substrate capacitance and thus avoid losses in it.

These new structures are beneficial in many applications. We experimentally demonstrate the benefits for a relatively small (6.6 cm) structure with a resonant frequency around 7 MHz by showing that it can transmit power two times as far as conventional resonant coils while maintaining above 80% efficiency. These structures are also beneficial in many other applications. For example, a higher-power and lower-frequency version of this structure designed for vehicle charging applications would have similar benefits in increasing the range and efficiency of WPT.

APPENDIX A
1-D PROXIMITY EFFECT CALCULATION

This section models the impact of eddy current loss on winding resistance assuming a 1-D field as described in Section II-A1. The eddy-current loss is caused by the time-varying magnetic flux density in the region of the winding, $B(t) = \hat{B} \cdot \sin(2\pi f \cdot t)$. The loss calculation is complicated

by the fact that the peak flux density is a function of the radius and vertical position as follows:

$$\hat{B}(r,z) = \frac{z}{h} \cdot \frac{\mu_0 \cdot \hat{I}_{\text{tot}}}{r \cdot \ln\left(\frac{r_2}{r_1}\right)} \tag{20}$$

where μ_0 is the permeability of free space, $\hat{I}_{\text{tot}}$ is the peak value of the total current, z is the vertical position from the bottom of the winding, and h is the height of the winding. Given that the loss is proportional to $\hat{B}^2$, we can use the average value of $\hat{B}^2$ over the volume of the winding. Averaging over the height, we find

$$\left\langle \hat{B}^2(r,z) \right\rangle_z = \frac{\int_0^h \hat{B}^2(r,z)\,dz}{h} = \frac{1}{3} \cdot \left(\frac{\mu_0 \cdot \hat{I}_{\text{tot}}}{r \cdot \ln\left(\frac{r_2}{r_1}\right)} \right)^2 \tag{21}$$

where $\langle \cdot \rangle_z$ indicates a spatial average over the elevation z. For the radius variation, we average over the area of the (r,φ) plane as follows:

$$\begin{aligned} \left\langle \hat{B}^2(r,z) \right\rangle &= \frac{\int_{r_1}^{r_2} \left\langle \hat{B}^2(r,z) \right\rangle_z 2\pi r dr}{\int_{r_1}^{r_2} 2\pi r dr} \\ &= \frac{1}{3} \cdot \left(\frac{\mu_0 \cdot \hat{I}_{\text{tot}}}{\ln\left(\frac{r_2}{r_1}\right)} \right)^2 \frac{\int_{r_1}^{r_2} \frac{1}{r} dr}{\int_{r_1}^{r_2} r dr} \\ &= \frac{\left(\mu_0 \cdot \hat{I}_{\text{tot}}\right)^2}{3 \cdot \ln\left(\frac{r_2}{r_1}\right)} \cdot \frac{2}{r_2^2 - r_1^2}. \end{aligned} \tag{22}$$

With this value of the average squared field amplitude, we can use the standard formula for eddy-currents in a lamination

$$P_e = \frac{\left\langle \hat{B}^2(r,z) \right\rangle \omega^2 t_c^2}{24\rho} V_f \tag{23}$$

where V_f is the total volume of foil. Because there are 2M layers of foil in the overlap region and M layers in region I, $V_f = \pi\left(r_2^2 - r_1^2\right) t_c M\left(1 + \theta/\pi\right)$. Substituting, we obtain the following:

$$\begin{aligned} P_e &= \frac{\left(\mu_0 \cdot \hat{I}_{\text{tot}}\right)^2}{3 \cdot \ln\left(\frac{r_2}{r_1}\right)} \frac{2\omega^2 t_c^2}{\left(r_2^2 - r_1^2\right) 24\rho} \pi\left(r_2^2 - r_1^2\right) tM \left(1 + \frac{\theta}{\pi}\right) \\ &= I_{\text{rms}}^2 \frac{\mu_0^2 \omega^2 t_c^3 \pi M}{18 \cdot \rho \cdot \ln\left(\frac{r_2}{r_1}\right)} \left(1 + \frac{\theta}{\pi}\right). \end{aligned} \tag{24}$$

The eddy-current loss is higher for a section of the resonant coil than for a simple loop, simply because there is larger amount of foil present in the high-frequency magnetic field. The factor by which this increases eddy-current loss is the last term in (24), and is equal to the factor by which the amount of conductor is increased: $k_2 = 1 + \frac{\theta}{\pi}$.

We can define a 1-D eddy-current resistance as follows:

$$R_e = \frac{{\mu_0}^2 \omega^2 t^3 \pi M}{18 \cdot \rho \cdot \ln\left(\frac{r_2}{r_1}\right)} \left(1 + \frac{\theta}{\pi}\right) \tag{25}$$

such that $P_e = I_{\text{rms}}^2 R_e$. A 1-D ac resistance factor defined as $F_{1dr} = \frac{R_{ac-1d}}{R_{\text{LF}}} = 1 + \frac{R_e}{R_{\text{LF}}}$ can now be evaluated, and is equal to

$$F_{1dr} = 1 + \frac{M^2}{9} \cdot \frac{{\mu_0}^2 \omega^2}{4\rho^2} t_c^4 \frac{k_2}{k_1}. \tag{26}$$

Substituting with skin depth $\delta = \sqrt{\frac{2\rho}{\mu_0 \omega}}$ yields

$$F_{1dr} = 1 + \frac{M^2}{9} \left(\frac{t_c}{\delta}\right)^4 \cdot \frac{k_2}{k_1}. \tag{27}$$

APPENDIX B
FEA EXTRACTION METHOD FOR THE FIELD WEAKENING FACTOR AND CURRENT CROWDING FACTORS

The field weakening and current crowding factors are extracted from a 2-D axis-symmetric FEA. Accurate modeling of the magnetic core properties and the physical dimensions is important to the result of the simulation. Each section of the modified self-resonant structure consists of two copper layers, so the FEA model is an inductor with 2m turns of foil. The foil layers of the model have equal current, and are driven with a sinusoidal current with a peak value $\hat{I}$ and an RMS value I_{rms}. The thickness of the foil windings is t_c, and the FEA mesh size within the winding must be at least five times smaller than t_c in order to accurately model the effects within the winding. Finally, a low frequency resistance of the FEA coil R_{lfea} is needed and is given by

$$R_{\text{lfea}} = \frac{4M\pi\rho}{\ln\left(\frac{r_2}{r_1}\right) t_c}. \tag{28}$$

The simulation assumes that the per-layer current is the same all the way around the 360° of the current path loop, whereas the actual resonant structure has current transferring between adjacent layers as the current flows around the loop, as shown in Fig. 4. Although this angular dependence affects the low-frequency resistance substantially, as captured by k_1 in (5), it has no significant effect on proximity-effect resistance. To demonstrate this, the FEA proximity effect resistance was found to be equal for two scenarios: first, for equal current sharing between every conductive layer ($\theta = 90°$ in Fig. 4) and second, current only in alternating layers ($\theta = 0°$ in Fig. 4).

A. Field Weakening Factor

The field weakening factor F_{fw} accounts for decreased proximity-effect loss due to a reduction in the magnetic field. The field weakening factor is

$$F_{\text{fw}} = \frac{\left\langle \hat{B}_{r,\text{fea}}^2 \right\rangle}{\left\langle \hat{B}_r^2 \right\rangle} = \frac{3\left\langle \hat{B}_{r,\text{fea}}^2 \right\rangle \ln\left(\frac{r_2}{r_1}\right)\left(r_2^2 - r_1^2\right)}{2\left(\mu_0 \cdot \hat{I}\right)^2} \tag{29}$$

where both $\langle \hat{B}^2_{r,\text{fea}} \rangle$ and $\langle \hat{B}^2_r \rangle$ are computed based on the inductor used in the FEA model. $\langle \hat{B}^2_{r,\text{fea}} \rangle$ is an FEA result, and is the spatial average of the square of the peak value of the magnetic field parallel to the foil layers. $\langle \hat{B_r}^2 \rangle$ is computed from (22), and is the calculated spatial average of the square of the peak value of the magnetic field assuming a 1-D magnetic field as described in Section II-A1.

B. Current Crowding Factor

The current crowding factor accounts for increased losses in the conductors due to horizontal current crowding. This factor is calculated from the resistance R_{fea} of the FEA model at the resonant frequency. We equate the calculated ESR of the FEA coil and R_{fea} as follows:

$$\begin{aligned} R_{\text{fea}} &= R_{\text{prox}} + F_{\text{cc}} R_{\text{lfea}} \\ &= F_{\text{fw}} \frac{(2M)^2}{9} \left(\frac{t_c}{\delta} \right)^4 R_{\text{lfea}} + F_{\text{cc}} R_{\text{lfea}} \end{aligned} \tag{30}$$

which results in a current crowding factor F_{cc} given by

$$F_{\text{cc}} = \frac{R_{\text{fea}} - R_{\text{prox}}}{R_{\text{lfea}}} = \frac{R_{\text{fea}}}{R_{\text{lfea}}} - \frac{F_{\text{fw}}(2M)^2}{9} \left(\frac{t_c}{\delta} \right)^4. \tag{31}$$

Appendix C
Loss in the High-Loss Substrate of the Modified Self-Resonant Structure

The high-loss PCB substrate used to support the thin conductive layers in the modified self-resonant structure does not significantly reduce the quality factor of the structure. The orientation ensures that the capacitance created through the substrate is not involved in the resonance of the structure, so the only loss is due to the displacement current induced by the leakage flux through the substrate. In our prototyping work, the loss in the substrate is 10^4 times smaller than the total loss.

As the first step toward determining the power loss in the substrates, we consider the substrate layer with the highest loss. In Fig. 7, this is the substrate that separates Layer 1 and Layer 2, and in general it is the substrate layer that is farthest away from the base of the pot core. The leakage flux between Layer 1 and Layer 2 does not vary with respect to radius, so therefore the magnetic field decreases with respect to the radius $H(r) = \frac{H_1 r_1}{r}$, where H_1 is the field at r_1 and r is the distance in the radial direction from the center of the pot core. If we assume that the field in the magnetic core is 0, then

$$\oint H \cdot dl = \int_{r_1}^{r_2} \frac{H_1 r_1}{r} dr = H_1 r_1 \ln \left(\frac{r_2}{r_1} \right) = I(t) \tag{32}$$

where $I(t)$ is the sum of the current in each section. The magnetic field at H_1 is found from (32), and is given by

$$H_1 = \frac{I(t)}{r_1 \ln \left(\frac{r_2}{r_1} \right)}. \tag{33}$$

The voltage across the substrate nearest the gap in the C-shape section is

$$V_{\text{rms}} = \frac{d\phi}{dt\sqrt{2}} = \mu_0 \omega t_s \left(\frac{I_{\text{rms}}}{\ln \left(\frac{r_2}{r_1} \right)} \right) \left(\frac{\pi - \theta}{2} + \theta \right) \tag{34}$$

where t_s is the thickness of the substrate and $\left(\frac{\pi - \theta}{2} + \theta \right)$ accounts for half the angle of overlap of the substrate. The voltage across the substrate linearly decreases around the C-shaped section until it reaches 0 at the midpoint; therefore, the power lost in the top section is

$$P_{\text{top}} = \frac{V^2_{\text{rms}}}{3R_{ps}}. \tag{35}$$

The equivalent parallel resistance of the section R_{ps} is

$$R_{ps} = \frac{1 + \sqrt{1 - 4D_s}}{2D_s \omega C_{\text{sub}}} \tag{36}$$

where D_s is the dissipation factor of the substrate. The substrate capacitance C_{sub} is

$$C_{\text{sub}} = \frac{\epsilon_s \pi (r_2^2 - r_1^2)}{t_s} \left(\frac{\pi - \theta}{2} + \theta \right) \tag{37}$$

where ϵ_s is the relative permittivity of the substrate material. The voltage on the substrate capacitance increases linearly with the section number; therefore, the total power lost in the high-loss substrate P_{sub} is

$$P_{\text{sub}} = \frac{P_{\text{top}} M}{3}. \tag{38}$$

Combining (34) and (35) into (38), the ESR due to the substrate loss R_{sub} is

$$\begin{aligned} R_{\text{sub}} &= \frac{M}{9R_{ps}} \left(\frac{\mu_0 \omega t_s \left(\frac{\pi - \theta}{2} + \theta \right)}{\ln \left(\frac{r_2}{r_1} \right)} \right)^2 \\ &= \frac{2D_s \omega^3 M \epsilon_s \mu_0^2 t_s \pi (r_2^2 - r_1^2) \left(\frac{\pi - \theta}{2} + \theta \right)^3}{9 \left(1 + \sqrt{1 - 4D_s} \right) \ln \left(\frac{r_2}{r_1} \right)^2}. \end{aligned} \tag{39}$$

In the prototyping work in this manuscript, a 25.4 μm thick polyimide substrate was used to support the thin foil layers. Polyimide has a D_s of approximately 0.0018, but the ESR arising from losses in the substrates was only 99.5 nΩ, which is four orders of magnitude smaller than the ESR of the structure. Equation (39) shows that substrate loss will be low for other designs as well. For example, a significant increase in the substrate thickness or the substrate dissipation factor will still cause an ESR well below the ESR of a typical structure.

References

[1] J. S. Ho *et al.*, "Wireless power transfer to deep-tissue microimplants," *Proc. Nat. Acad. Sci.*, vol. 111, no. 22, pp. 7974–7979, 2014.

[2] M. Adeeb, A. Islam, M. Haider, F. Tulip, M. Ericson, and S. Islam, "An inductive link-based wireless power transfer system for biomedical applications," *Active Passive Electron. Compon.*, vol. 2012, 2012, Art. no. 879294.

[3] A. P. Sample, D. A. Meyer, and J. R. Smith, "Analysis, experimental results, and range adaptation of magnetically coupled resonators for wireless power transfer," *IEEE Trans. Ind. Electron.*, vol. 58, no. 2, pp. 544–554, Feb. 2011.
[4] T. Imura, H. Okabe, and Y. Hori, "Basic experimental study on helical antennas of wireless power transfer for electric vehicles by using magnetic resonant couplings," in *Proc. IEEE Vehicle Power Propulsion Conf.*, 2009, pp. 936–940.
[5] E. Waffenschmidt and T. Staring, "Limitation of inductive power transfer for consumer applications," in *Proc. 13th Euro. Conf. Power Electron. Appl.*, 2009, pp. 1–10.
[6] M. Kesler, "Highly resonant wireless power transfer: Safe efficient, and over distance," Witricity Corporation, Watertown, MA, USA, pp. 1–32, 2013.
[7] C. R. Sullivan, B. A. Reese, A. L. F. Stein, and P. A. Kyaw, "On size and magnetics: Why small efficient power inductors are rare," in *Proc. Int. Symp. 3D Power Electron. Integration Manufacturing*, 2016, pp. 1–23.
[8] D. J. Perreault *et al.*, "Opportunities and challenges in very high frequency power conversion," in *Proc. 24th Annu. Appl. Power Electron. Conf. Expo.*, 2009, pp. 1–14.
[9] K. Fotopoulou and B. W. Flynn, "Wireless power transfer in loosely coupled links: Coil misalignment model," *IEEE Trans. Mag.*, vol. 47, no. 2, pp. 416–430, Feb. 2011.
[10] C. Florian, F. Mastri, R. P. Paganelli, D. Masotti, and A. Costanzo, "Theoretical and numerical design of a wireless power transmission link with GaN-based transmitter and adaptive receiver," *IEEE Trans. Microw. Theory Techn.*, vol. 62, no. 4, pp. 931–946, Apr. 2014.
[11] A. Khripkov, W. Hong, and K. Pavlov, "Design of an integrated resonant structure for wireless power transfer and data telemetry," in *Proc. IEEE MTT-S Int. Microw. Workshop Ser. RF Wireless Technol. Biomed. Healthcare Appl.*, 2013, pp. 1–3.
[12] A. Kurs, A. Karalis, R. Moffatt, J. D. Joannopoulos, P. Fisher, and M. Soljačić, "Wireless power transfer via strongly coupled magnetic resonances," *Science*, vol. 317, no. 5834, pp. 83–86, 2007.
[13] S.-H. Lee and R. D. Lorenz, "Development and validation of model for 95%-efficiency 220 watt wireless power transfer over a 30-cm air gap," *IEEE Trans. Ind. Appl.*, vol. 47, no. 6, pp. 2495–2504, Nov./Dec. 2011.
[14] C. R. Sullivan, "Cost-constrained selection of strand diameter and number in a Litz-wire transformer winding," *IEEE Trans. Power Electron.*, vol. 16, no. 2, pp. 281–288, Mar. 2001.
[15] C. R. Sullivan and L. Beghou, "Design methodology for a high-Q self-resonant coil for medical and wireless-power applications," in *Proc. IEEE 14th Workshop Control Modeling Power Electron.*, 2013, pp. 1–8.
[16] J. A. Ferreira and J. D. Van Wyk, "Electromagnetic energy propagation in power electronic converters: Toward future electromagnetic integration," *Proc. IEEE*, vol. 89, no. 6, pp. 876–889, Jun. 2001.
[17] J. T. Strydom and J. D. Van Wyk, "Volumetric limits of planar integrated resonant transformers: A 1 MHz case study," *IEEE Trans. Power Electron.*, vol. 18, no. 1, pp. 236–247, Jan. 2003.
[18] E. Waffenschmidt and J. Ferreira, "Embedded passives integrated circuits for power converters," in *Proc. IEEE 33rd Power Electron. Specialists Conf.*, vol. 1, 2002, pp. 12–17.
[19] Q. Li and Y. C. Liang, "An inductive power transfer system with a high-q resonant tank for mobile device charging," *IEEE Trans. Power Electron.*, vol. 30, no. 11, pp. 6203–6212, Nov. 2015.
[20] A. L. F. Stein, P. A. Kyaw, and C. R. Sullivan, "High-Q self-resonant structure for wireless power transfer," in *Proc. IEEE Appl. Power Electron. Conf. Expo.*, 2017, pp. 3723–3729.
[21] R. Marques, J. Martel, F. Mesa, and F. Medina, "Left-handed-media simulation and transmission of EM waves in subwavelength split-ring-resonator-loaded metallic waveguides," *Phys. Rev. Lett.*, vol. 89, no. 18, 2002, Art. no. 183901.
[22] T. Oh and B. Lee, "Analysis of wireless power transfer using metamaterial slabs made of ring resonators at 13.56 MHz," *J. Electromag. Eng. Sc.*, vol. 13, no. 4, pp. 259–262, 2013.
[23] P. A. Kyaw, A. L. F. Stein, and C. R. Sullivan, "High-Q resonator with integrated capacitance for resonant power conversion," in *Proc. IEEE Appl. Power Electron. Conf. Expo.*, 2017, pp. 2519–2526.
[24] P. A. Kyaw, A. L. F. Stein, and C. R. Sullivan, "Power density optimization of resonant tanks using standard capacitors," in *Proc. IEEE 18th Workshop Control Modeling Power Electron.*, 2017, pp. 1–7.
[25] B. X. Foo, A. L. Stein, and C. R. Sullivan, "A step-by-step guide to extracting winding resistance from an impedance measurement," in *Proc. IEEE Appl. Power Electron. Conf. Expo.*, 2017, pp. 861–867.
[26] P. A. Kyaw, A. L. Stein, and C. R. Sullivan, "Power handling capability of self-resonant structures for wireless power transfer," in *Proc. IEEE PELS Workshop Emer. Technol., Wireless Power (WoW)*, 2018, pp. 1–6.
[27] A. L. Stein, P. A. Kyaw, and C. R. Sullivan, "The feasibility of self-resonant structures in wireless power transfer applications," in *Proc. IEEE PELS Workshop Emer. Technol.: Wireless Power (WoW)*, 2018, pp. 1–6.

Aaron L. F. Stein received the Ph.D. degree in electrical engineering and computer science from the University of Michigan, Ann Arbor, MI, USA, in 2016.

He is currently a Postdoctoral Research Associate with Dartmouth College, Hanover, NH, USA. He has authored or coauthored technical papers on topics including wireless power transfer, energy harvesting, and electromagnetic components.

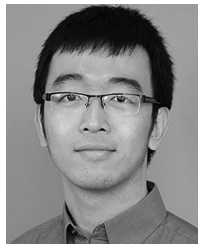

Phyo Aung Kyaw (S'15) received the B.A. degree in physics from Amherst College, Amherst, MA, USA, in 2014. He is currently working toward the Ph.D. degree in electrical engineering at Dartmouth College, Hanover, NH, USA.

His research interests include power electronics and magnetics, electromagnetic and piezoelectric resonators, high-frequency passive components, and wireless power transfer.

Charles R. Sullivan (S'93–M'96–SM'12–F'14) received the B.S.(Hons.) degree in electrical engineering from Princeton University, Princeton, NJ, USA, in 1987, and the Ph.D. degree in electrical engineering from the University of California, Berkeley, CA, USA, in 1996.

Between the B.S. and Ph.D. degrees, he was with Lutron Electronics designing electronic ballasts. He is currently a Professor with the Thayer School of Engineering at Dartmouth, Hanover, NH, USA. His research interests include design optimization of magnetics for power applications, energy efficiency, and renewable energy, and electromagnetic modeling of capacitors.

Dr. Sullivan was the recipient of the National Science Foundation CAREER Award and two Power Electronic Society Prize Paper Awards.